SHORT COMMUNICATION

MR simulation for prostate radiation therapy: effect of coil mounting position on image quality

[1]J SUN, MSc, [2]P PICHLER, B.App.Sc (MRT), [3]J DOWLING, PhD, [1]F MENK, PhD, [4]P STANWELL, PhD, [5]J ARM, MSc and [1,2]P B GREER, PhD

[1]School of Mathematical and Physical Sciences, University of Newcastle, Newcastle, NSW, Australia
[2]Department of Radiation Oncology, Calvary Mater Newcastle, Newcastle, NSW, Australia
[3]Commonwealth Scientific and Industrial Research Organisation (CSIRO) Australian e-Health Research Centre, Brisbane, QLD, Australia
[4]School of Health Sciences, University of Newcastle, Newcastle, NSW, Australia
[5]Hunter New England Health, Newcastle, NSW, Australia

Address correspondence to: Mr Jidi Sun
E-mail: *jidi.sun@uon.edu.au*

Objective: To eliminate the effects of body deformation for MR-based prostate treatment planning, coil mounts are essential. In this study, we evaluated the effect of the coil set-up on image quality.

Methods: A custom-designed pelvic-shaped phantom was scanned by systematically increasing the anterior body-to-coil (BTC) distance from 30 to 90 mm. The image quality near the organs of interest was determined in order to characterize the relationship between image quality and BTC distance at the critical organ structures. The half intensity reduction (HIR) was calculated to determine the sensitivity of each organ structure to the BTC distance change.

Results: As the BTC distance increased, the uniformity reduced at 3% per millimetre. The HIR value indicated that the bladder signal is most sensitive to the change in BTC distance. By maintaining a constant BTC distance set-up, the intensity uniformity was improved by 28% along the B0 directions.

Conclusion: Positioning the MRI coil on mounts can reduce body deformation but adversely degrades the image quality. The magnitude of this effect has been quantified for prostate MR simulation scanning. The coil needs to be positioned not only with a minimal but also uniform BTC distance in order to maximize image quality.

Advances in knowledge: A method to characterize the effect on image quality due to the use of coil mounts was demonstrated. Coil mounts whose height can be adjusted individually to keep BTC distance constant are necessary to maintain a uniform image across the entire field of view.

Compared with CT images, MR images have superior soft tissue contrast, which increases the organ delineation accuracy. There is growing interest in the use of MR as the sole imaging modality for radiation therapy planning, with the increasing installation of MR scanners in radiation therapy departments and the development of MR linac devices.[1–3] However, several factors limit the use of MRI as the sole modality for radiotherapy treatment planning. These not only include spatial distortion[4–6] and lack of electron density[7–10] but also the anatomy variation due to differences in patient positioning set-up on MR scanner from the treatment position. Khoo et al[11] proposed that in order to apply MR scans to the radiotherapy, patient set-up on the MR scanner table needs to reproduce the one on the treatment table. For current scanners with a flat table top, patient positioning is mainly affected by the surface coil that is conventionally attached to the patient's pelvis, deforming the anterior external body contour.

For the prostate scan, the anterior body deformation owing to coil compression can be eliminated by using a coil mount to lift the coil above the body. Kapanen et al[12] implemented a home-made coil mount to hold the coil above the body. They assessed the effect of their coil mount on spatial distortion. To simulate a flat treatment table, McJury et al[13] inserted a flat panel onto the scanner in order to eliminate the posterior body deformation. They showed that by inserting a flat couch to their curved table top, the signal-to-noise ratio (SNR) in an oil-filled phantom decreased by 14%.[13] To our knowledge, no systematic study has been conducted on the effect on image quality of lifting the coil above the scanned body using coil mounts. It is important to understand what effect these new coil positioning devices have on image quality and how best to utilize these devices for MR-based treatment planning to obtain optimal image quality.

This study aims to determine the effect on image quality of using commercial coil mounts to lift the surface coil above

Figure 1. Schematic diagrams of the anthropomorphic phantom in transverse view (a). Larger diagram in (b) shows the sagittal view and smaller diagram shows the transverse view of grid-phantom. A photo of coil mounts (c). Two coil mount set-ups are shown in (d) and (e), horizontal set-up and parallel set-up, respectively, where the main magnetic field (B0) direction indicates the phantom set-up on scanner. A flat table was used in this study.
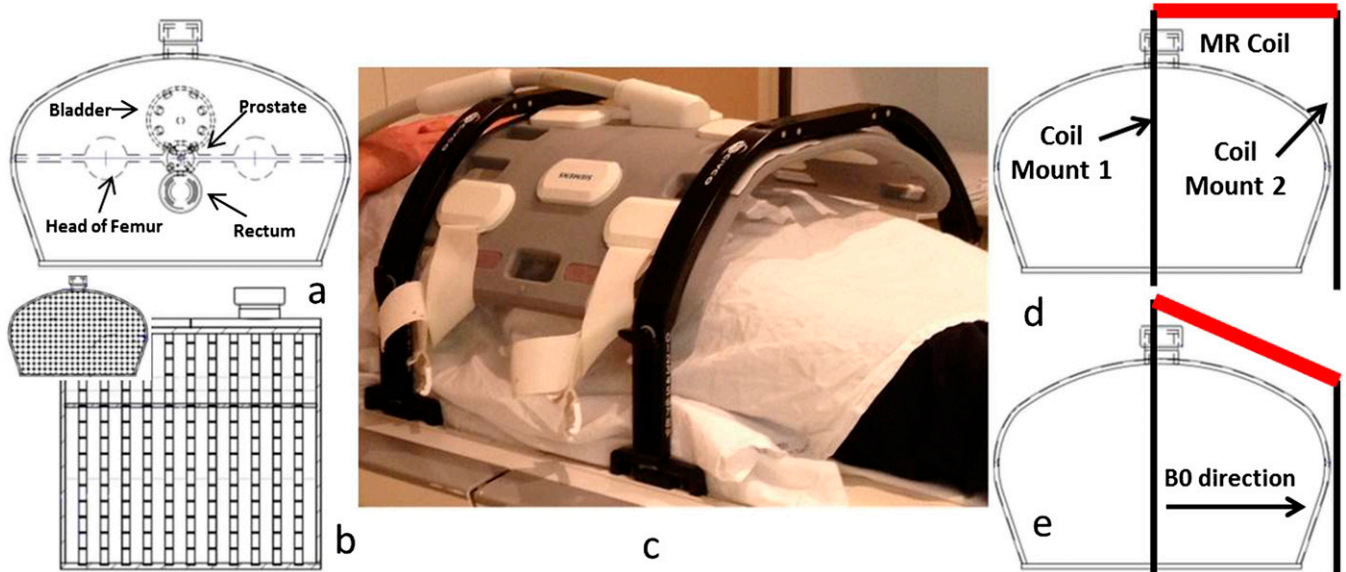
the pelvis for prostate radiation therapy MR scanning. The effect of both variation in body-to-coil (BTC) distance along the main magnetic field (B0) direction and increase in BTC distance in the anteroposterior (AP) direction are systematically examined using specially constructed pelvic-shaped MR test phantoms. The findings will assist with clinical implementation of these devices for MR-based planning and inform future design of these devices.

METHODS AND MATERIALS
Phantom design
Two phantoms were custom manufactured to the shape of a human pelvis, with the external surface made of polymethylmethacrylate. One of the phantoms is an anthropomorphic phantom ("anthro-phantom") containing all the organs of interest in surrogate structures (Figure 1a). The location and size of these structures were based on average results from 39 patient CT scans by Lambert et al.[10] The prostate and bladder structures inside the anthro-phantom are shaped by hollow plastic spheres, with holes drilled through the surface allowing liquid to fill the structure. The rectum is a cylindrical pipe filled with air, while the head of the femur is a solid plastic sphere. This phantom was used to estimate the image quality change near region of interest (ROI) structures when the BTC distance varied.

The second phantom ("grid-phantom") has the same external body dimension but with 11 plastic grid sheets positioned approximately 20 mm apart and parallel to each other (Figure 1b). This grid-phantom was originally designed for quantifying the geometric distortion of a pelvic-sized MR image. In this study, the grid-phantom was used to evaluate the image quality variation caused by different coil positioning set-ups. Image profiles were sampled at the spaces between adjacent grid sheets to give continuous image quality variation.

Both phantoms were filled with mineral oil instead of water in order to avoid the standing wave artefact in our 3-T scanner.

Figure 2. Intensity map of the sagittal image acquired with horizontal set-up (a) as shown in Figure 1d and parallel set-up (b) as shown in Figure 1e, and the pixel-by-pixel-based percentage intensity difference (c). The coil orientation is illustrated by the white line. The arrows indicate the region of most signal loss.
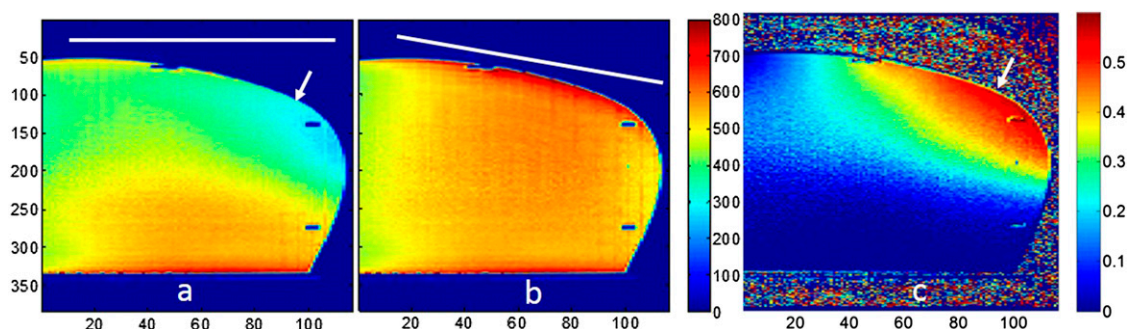
Both phantoms have a 25-mm thick filling cap mounted to the anterior surface for filling with oil. Because the cap was partially screwed on to reduce the pressure within the phantom, the minimally achievable BTC distance is approximately 30 mm.

MR sequence and scans

A Magnetom® Skyra 3-T MR scanner (Siemens Healthcare, Erlangen, Germany) was used for scanning. The body array coil was used (18 channel body matrix coil; Siemens Healthcare). The body matrix coil is a high density surface coil, with three clusters of six elements to improve the SNR and allow increased acceleration factors. It can also be used in combination with a 32-channel spine array that yields up to 60 elements in a single field of view (FOV). The scanner has a dedicated radiation therapy flat table top (CIVCO Medical Solutions, Orange City, IA). A three dimensional (3D) turbo spin echo (TSE) volumetric T_2 weighted sequence was used, and the parameters are repetition time, 1200 ms; echo time, 101 ms; α, 135°; bandwidth, 505 Hz per pixel; echo train length, 61; pixel size, 1 mm; slice thickness, 2 mm; and FOV, $320 \times 320 \times 240$ mm^3. The TSE with 90° longitudinal flip-back pulse (RESTORE, Siemens Healthcare) was applied to increase the longitudinal magnetization, so the fluid intensity could be improved. A large FOV was used to include the entire phantom. To minimize effects on image quality owing to factors other than the coil set-up, spatial distortion was corrected using the vendor-provided 3D algorithm, and the image intensity homogeneity was enhanced with the pre-scan normalize filter (Siemens Healthcare). To achieve patient positioning and external contour consistency between the MR scanner and the linear accelerator treatment table, commercial coil mounts (CIVCO Medical Solutions) were used to hold the surface coil off the phantom (Figure 1c). The height of individual coil mount was adjusted independently. Details of the phantom and coil positioning are given in the following sections.

Body-to-coil distance (B0 direction variation)

In the supine position, the anterior pelvic body contour descends along the B0 direction. Unlike the home-made coil mount used by Kapanen et al,[12] the commercial coil mounts used in this study have the ability to adjust the height of the superior and inferior individual mounts independently. This allows the BTC distance to be more consistent along the B0 direction.

The grid-phantom was positioned as shown in Figure 1d,e. The coil mounts were positioned in the following two orientations: (1) both coil mounts were kept at the same height to simulate the set-up used in Kapanen et al,[12] identified as horizontal set-up (Figure 1d) and (2) the height of the coil mounts were adjusted so that the BTC distance was kept as uniform as possible along the B0 direction, identified as parallel set-up (Figure 1e). There are 11 grid sheets inside the distortion phantom, so 12 sagittal images were sampled every 20 mm at the intermediate spaces between the grid sheets where only oil is presented. The intensity uniformity was determined on each sagittal image, using the American College of Radiology (ACR) procedure (a 1-cm^2 circular ROI was placed at the highest and lowest signal region) and recommended criterion (82%) as the guide.[14]

Figure 3. Intensity uniformity against estimated body-to-coil (BTC) distances for horizontal set-up and parallel set-up images. Black line indicates the recommended criterion for the American College of Radiology (ACR) MRI quality assurance phantom. The uniformity degraded below the ACR criterion after around 40-mm BTC distance. Hori, horizontal; para, parallel.
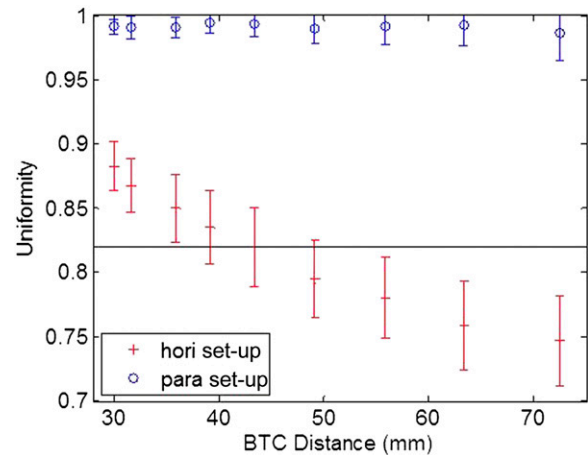
Along the B0 direction, nine transverse images were sampled every approximately 80 mm to give images with slightly different BTC distances. The intensity uniformity was calculated using the formula stated in Equation (1), where I_{max} and I_{min} are the mean signals of the regions with the highest and lowest signals, respectively.[14] Because the body coil is invisible on the MR image, the physical BTC distance cannot be established directly. The estimated BTC distance is the sum of the minimally achievable BTC distance (30 mm) and the relative

Figure 4. Image acquired with 30 to 90-mm anterior body-to-coil distance (all images have the same intensity window setting). Only the bladder and rectum are shown on these images.
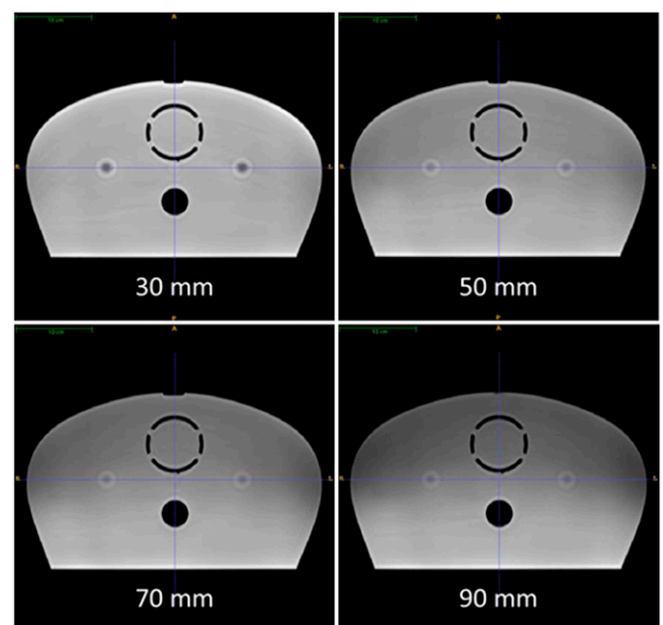
phantom height change (phantom height difference on two adjacent transverse images).

$$\text{Uniformity} = 1 - \frac{I_{\max} - I_{\min}}{I_{\max} + I_{\min}} \qquad (1)$$

Body-to-coil distance (anteroposterior direction variation)

The anthro-phantom was used to provide the spatial information of the organs of interest. The height of the coil mounts was systematically increased in increments of 20 mm to give the physical BTC distances from 30 to 90 mm. ROIs were contoured on the 30-mm BTC image because of its superior image quality, and the same contours were copied to the other images.

The SNR within the ROI was used as the image quality metric, and it was defined as the ratio of the mean ROI signal to the background noise.[15] The SNR was then plotted against the BTC distance and the data were fitted with an exponential regression as $\text{SNR} = \text{SNR}_0\exp^{-kx}$, where k is the decay rate and x is the BTC distance. The half intensity reduction (HIR) is calculated using the decay rate in Equation (2):

$$\text{HIR} = \frac{\ln(2)}{k} \qquad (2)$$

The term HIR is introduced to represent the BTC distance when the SNR in a particular organ structure is halved. Low HIR value indicates more sensitivity to the BTC distance change.

RESULTS
Body-to-coil distance (B0 direction variation)
Figure 2 shows the intensity distributions for both set-ups and the percentage differences. As the BTC distance increased, the horizontal set-up image lost as much as 50% of the intensity at the anterior region compared with the parallel set-up image. The uniformity on the horizontal set-up image was 70% ± 6%, which failed the ACR recommended criterion, while the parallel set-up improved the uniformity to 98% ± 1%. The parallel set-up uniformity remains >95% along the B0 direction on Figure 3, whereas the horizontal set-up uniformity decays by 3% per millimetre after applying the exponential regression.

Body-to-coil distance (anteroposterior direction variation)
A noticeable signal drop near the phantom's anterior region was observed in Figure 4 after increasing the BTC distance. Figure 5 plots the organ structure SNR variation against the BTC distance change. The decay rate of each organ structure correlates with the organ geometric location. Table 1 quantifies the HIR value obtained from Figure 5. The BTC distance has more influence on the signal at the structures close to the anterior region (*e.g.* bladder) than the signal for the structures close to the posterior region (*e.g.* rectum).

DISCUSSION
In this work, we found that the uniformity within the phantom reduced by 3% per millimetre as the BTC distance increased. Additionally, by maintaining constant BTC distance along the B0

Figure 5. Plot of the signal-to-noise ratio (SNR) of regions of interest contoured on images acquired with different body-to-coil (BTC) distances. The exponential regression was applied to find the decay rate and half intensity reduction in Table 1. LHOF, left head of femur; RHOF, right head of femur.

direction, the image uniformity improved from 70% ± 6% to 98% ± 1% along the B0 direction. In order to eliminate the coil-induced external body contour deformation, coil mounts are necessary for MR-based planning. At the same time, in order to achieve uniform intensity images, the coil mounts should be adjusted based on the patient's external anatomical geometry and a constant BTC distance throughout the B0 direction should be maintained. As the waist size of the patient increases, the difference between the AP contour height (above the table) near the superior and inferior ends will increase. The image quality improvement of conforming the coil to the external body will be more important in these cases. It should be noted that the vendor, size of the elements in the receive coil and the scan sequence will affect the image quality result (*e.g.* uniformity), thus the result may vary slightly by manufacturer or coil selection. However, for similar pelvic scans (acquired with both posterior and anterior surface coils), we believe that it is essential to minimize the BTC distance and to maintain a constant BTC distance in order to improve the image quality.
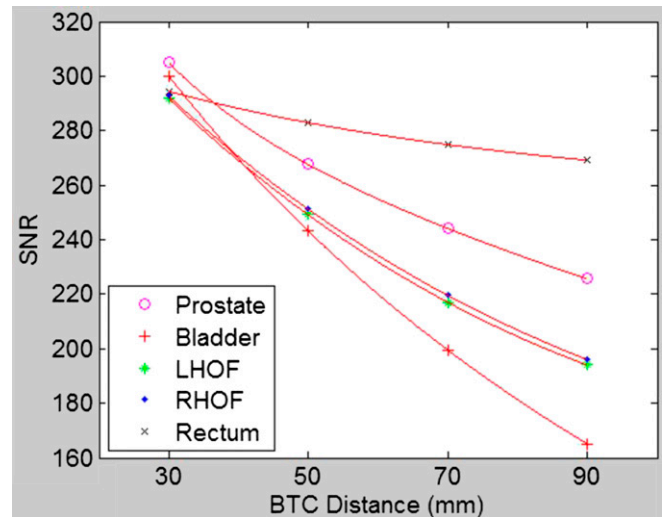
One improvement of the set-up is to attach a long object that is visible on the MR image to the inside surface of the coil. This

Table 1. Exponential regression of the data in Figure 5

k (×10^{-3})	k	HIR (mm)
Prostate	5.1	136
Bladder	10.0	69
LHOF	6.9	100
RHOF	6.8	102
Rectum	1.5	462

HIR, half intensity reduction; LHOF, left head of femur; RHOF, right head of femur.
The HIR distance is calculated from the decay rate (k).

has two advantages: firstly, because the object is attached directly to the coil, the BTC distance is minimal. Therefore, the object provides the reference intensity along the B0 direction. This reference intensity can be used to compare the mean intensity at different organ-of-interest locations. The second advantage is that the physical BTC distance can be established using the visible object to give the actual image quality and BTC distance correlation.

Finally, it would be useful to determine the image quality variation between scans, and this can be carried out by acquiring repetitive images. However, as this work mainly concentrates on the image quality effect of different coil set-ups, and these set-ups induce more influence on the image quality than the scanner performance variation, the later factor is insignificant.

In conclusion, in order to maintain a uniform image along all directions, the coil needs to be positioned not only with minimal BTC distance but also parallel to the phantom surface. By systematically increasing the BTC distance, we found that among all organs of interest, the bladder is the most sensitive to the anterior BTC distance change.

REFERENCES

1. Lagendijk JJ, Raaymakers BW, Raaijmakers AJ, Overweg J, Brown KJ, Kerkhof EM, et al. MRI/linac integration. *Radiother Oncol* 2008; **86**: 25–9. doi: 10.1016/j.radonc.2007.10.034

2. Greer PB, Dowling JA, Lambert JA, Fripp J, Parker J, Denham JW, et al. A magnetic resonance imaging-based workflow for planning radiation therapy for prostate cancer. *Med J Aust* 2011; **194**: S24–7.

3. Burke B, Ghila A, Fallone BG, Rathee S. Radiation induced current in the RF coils of integrated linac-MR systems: the effect of buildup and magnetic field. *Med Phys* 2012; **39**: 5004–14. doi: 10.1118/1.4737097

4. Tanner SF, Finnigan DJ, Khoo VS, Mayles P, Dearnaley DP, Leach MO. Radiotherapy planning of the pelvis using distortion corrected MR images: the removal of system distortions. *Phys Med Biol* 2000; **45**: 2117–32.

5. Wang D, Doddrell DM, Cowin G. A novel phantom and method for comprehensive 3-dimensional measurement and correction of geometric distortion in magnetic resonance imaging. *Magn Reson Imaging* 2004; **22**: 529–42. doi: 10.1016/j.mri.2004.01.008

6. Chen L, Price RA Jr, Wang L, Li J, Qin L, McNeeley S, et al. MRI-based treatment planning for radiotherapy: dosimetric verification for prostate IMRT. *Int J Radiat Oncol Biol Phys* 2004; **60**: 636–47. doi: 10.1016/j.ijrobp.2004.05.068

7. Jonsson JH, Karlsson MG, Karlsson M, Nyholm T. Treatment planning using MRI data: an analysis of the dose calculation accuracy for different treatment regions. *Radiat Oncol* 2010; **5**: 62. doi: 10.1186/1748-717X-5-62

8. Johansson A, Karlsson M, Nyholm T. CT substitute derived from MRI sequences with ultrashort echo time. *Med Phys* 2011; **38**: 2708–14.

9. Dowling JA, Lambert J, Parker J, Salvado O, Fripp J, Capp A, et al. An atlas-based electron density mapping method for magnetic resonance imaging (MRI)-alone treatment planning and adaptive MRI-based prostate radiation therapy. *Int J Radiat Oncol Biol Phys* 2012; **83**: e5–11. doi: 10.1016/j.ijrobp.2011.11.056

10. Lambert J, Greer PB, Menk F, Patterson J, Parker J, Dahl K, et al. MRI-guided prostate radiation therapy planning: Investigation of dosimetric accuracy of MRI-based dose planning. *Radiother Oncol* 2011; **98**: 330–4. doi: 10.1016/j.radonc.2011.01.012

11. Khoo VS, Dearnaley DP, Finnigan DJ, Padhani A, Tanner SF, Leach MO. Magnetic resonance imaging (MRI): considerations and applications in radiotherapy treatment planning. *Radiother Oncol* 1997; **42**: 1–15.

12. Kapanen M, Collan J, Beule A, Seppälä T, Saarilahti K, Tenhunen M. Commissioning of MRI-only based treatment planning procedure for external beam radiotherapy of prostate. *Magn Reson Med* 2013; **70**: 127–35.

13. McJury M, O'Neill A, Lawson M, McGrath C, Grey A, Page W, et al. Assessing the image quality of pelvic MR images acquired with a flat couch for radiotherapy treatment planning. *Br J Radiol* 2011; **84**: 750–5. doi: 10.1259/bjr/27295679

14. *Phantom test guidance for the ACR MRI accreditation program*. Reston, VA: American College of Radiology; 2005.

15. Bao Q, Chatziioannou AF. Estimation of the minimum detectable activity of preclinical PET imaging systems with an analytical method. *Med Phys* 2010; **37**: 6070–83.